Foot-terrain Deformation based Parameters Identification of MuJoCo for Simulation of Bipedal Locomotion on Deformable Terrain

Sunil Gora[1] and Ashish Dutta[2]

***Abstract*— Biped locomotion on deformable terrain is challenging due to the need for accurately modeling the terrain deformation during walk. In this paper, we analyze the solver parameters of the sphere-plane collision model for a biped robot walk on deformable terrain. The static equilibrium deformation of the terrain is used to identify these parameters, which are further corrected using the robot's inverse dynamics to simulate bipedal locomotion on deformable terrain.**

I. INTRODUCTION

Legged locomotion is an active area of robotics research due to its ability to traverse rugged terrain. Most past research has focused on traversing flat terrain and assumed rigid contact between the foot and the terrain [1]. On unstructured outdoor terrains, such as grass, sand, and soft clay, the terrain deformation significantly affects the dynamic balancing of the robot. This terrain deformation is neglected in the COM motion generated by LIPM or NIP model with rigid contact constraint. Xiong et al. [2] analyzed the stability region on deformable granular terrain from the static stability of COM. Mesesan et al. [3] stabilized the stance foot of the TORO robot using a damping wrench for walking on deformable terrain. Gora et al. [4] included the terrain deformation in the simplified dynamics model, and proposed three-dimensional walking pattern generation on deformable terrain using spherical inverted pendulum (SIP) in the SSP and suspended pendulum in the DSP [5]. A linear spring-damper contact model is used to consider the terrain deformation in the simplified dynamics model.

Acosta et al. [6] used experimental data to identify the stiffness and damping of MuJoCo and compared the accuracy with that of the Drake and Bullet simulators. In this paper, we analyze the solver parameters for the sphere-plane collision model in MuJoCo. The static equilibrium deformation of the terrain is used to identify these parameters, which are corrected using the robot's inverse dynamics to simulate bipedal locomotion on deformable terrain.

II. DYNAMIC MODELING OF HUMANOID ROBOT

The humanoid robot is modeled as a floating-base system, with the floating-base frame attached to the center of the hip link as shown in Fig. 1. The position and orientation of the floating-base are denoted by the vector $\boldsymbol{q}_0$, and the actuated joint coordinates are denoted by the vector $\boldsymbol{q}_\theta$. The dynamics

*All Authors are with the Department of Mechanical Engineering, Indian Institute of Technology Kanpur, India. Email: [1] sunilgora.sg@gmail.com, [2] adutta@iitk.ac.in

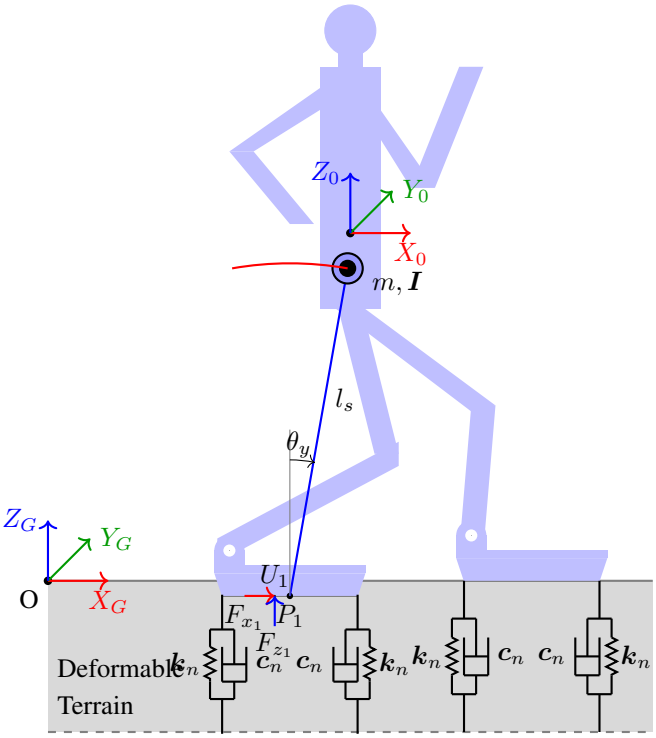

Fig. 1: Humanoid robot with foot-terrain interaction model

of the robot can be written as

$$\begin{bmatrix} \boldsymbol{I}_0 & \boldsymbol{I}_{0\theta} \\ \boldsymbol{I}_{0\theta}^T & \boldsymbol{I}_\theta \end{bmatrix} \begin{bmatrix} \ddot{\boldsymbol{q}}_0 \\ \ddot{\boldsymbol{q}}_\theta \end{bmatrix} + \begin{bmatrix} \boldsymbol{c}_0 \\ \boldsymbol{c}_\theta \end{bmatrix} = \begin{bmatrix} \boldsymbol{0} \\ \boldsymbol{\tau}_\theta \end{bmatrix} + \sum_{i=1}^{e_n} \begin{bmatrix} \boldsymbol{J}_{i_0}^T \\ \boldsymbol{J}_{i_\theta}^T \end{bmatrix} \boldsymbol{w}_i. \quad (1)$$

Here, $\boldsymbol{I}_0 \in \mathbb{R}^{6\times6}$ and $\boldsymbol{I}_\theta \in \mathbb{R}^{22\times22}$ are the inertia matrices of the base and links, respectively, $\boldsymbol{I}_{0\theta} \in \mathbb{R}^{6\times22}$ is the coupling inertia matrix, $\boldsymbol{c}_0 \in \mathbb{R}^{6\times1}$ and $\boldsymbol{c}_\theta \in \mathbb{R}^{22\times1}$ are the vectors of position and velocity-dependent terms associated with the base and links, respectively, $\boldsymbol{\tau}_\theta \in \mathbb{R}^{22\times1}$ is the joint torques vector, $\boldsymbol{J}_{i_0} \in \mathbb{R}^{6\times6}$ and $\boldsymbol{J}_{i_\theta} \in \mathbb{R}^{6\times22}$ are the Jacobian matrices, which map the joint coordinates of the base and links, respectively to the angular and linear velocity of i^{th} contact point, $\boldsymbol{w}_i \in \mathbb{R}^{6\times1}$ is the wrench vector acting at i^{th} contact point, and e_n is the number of points where the contact force is acting on the robot.

III. CONTACT DYNAMICS OF FOOT ON DEFORMABLE TERRAIN

The foot-terrain interaction model is crucial for locomotion on deformable terrain, as terrain deformation significantly affects the robot's dynamic balance [7]. Linear spring-damper contact models are commonly used for simulating

robotic systems due to their simplicity [8]. The foot-terrain interaction modeled with the normal spring-damper contact model is illustrated in Fig. 1. The nonlinear contact model, such as the Hunt-Crossley model, is also used to simulate the contact forces of the foot-terrain interaction on deformable terrain [9]. MuJoCo physics engine uses a nonlinear optimization-based contact model [10]. The default solver parameters of MuJoCo are analyzed for the sphere-plane collision model and modified to simulate bipedal locomotion on deformable terrain.

A. MuJoCo's optimization-based contact model

For the reader's understanding, we are reproducing MuJoCo's contact formulation in terms of the variables used in the source code [10]. In MuJoCo physics engine, next state velocities $\dot{\boldsymbol{q}}(t+h)$ in discrete time for forward dynamics simulation of timestep h are given by

$$\dot{\boldsymbol{q}}(t+h) = \dot{\boldsymbol{q}}(t) + \boldsymbol{M}^{-1}((\boldsymbol{\tau} - \boldsymbol{c})h + \boldsymbol{J}^T\boldsymbol{f}). \tag{2}$$

Here, $\dot{\boldsymbol{q}}(t)$ is the vector of current state velocities, $\boldsymbol{M}$ is the mass moment of inertia matrix, $\boldsymbol{\tau}$ is the vector of joint actuation torques, $\boldsymbol{c}$ is the vector of Coriolis and centrifugal forces, $\boldsymbol{J}$ is the constraint Jacobian, and $\boldsymbol{f}$ is the contact impulse. By multiplying with Jacobian $\boldsymbol{J}$, contact-space dynamics is written as

$$\boldsymbol{v}^+ = \boldsymbol{v}^- + \boldsymbol{A}\boldsymbol{f}, \tag{3}$$

where,

$$\boldsymbol{v}^+ = \boldsymbol{J}\dot{\boldsymbol{q}}(t+h), \tag{4}$$

$$\boldsymbol{v}^- = \boldsymbol{J}(\dot{\boldsymbol{q}}(t) + h\boldsymbol{M}^{-1}(\boldsymbol{\tau} - \boldsymbol{c})), \tag{5}$$

$$\boldsymbol{A} = \boldsymbol{J}\boldsymbol{M}^{-1}\boldsymbol{J}^T. \tag{6}$$

The contact impulse $\boldsymbol{f}$ is solved using a convex optimization problem, which minimizes the kinetic energy in contact-space subject to friction-cone constraints, i.e.,

$$\begin{aligned} \min_{\mathbf{f}} \quad & (\boldsymbol{v}^+ - \boldsymbol{v}^*)^T\boldsymbol{A}^{-1}(\boldsymbol{v}^+ - \boldsymbol{v}^*) + \boldsymbol{f}^T\boldsymbol{R}\boldsymbol{f}, \\ \text{s.t.} \quad & \mu^2 f_{i_z}^2 - f_{i_y}^2 - f_{i_x}^2 \geq 0, \\ & f_{i_z} \geq 0. \end{aligned} \tag{7}$$

The kinetic energy is measured relative to a desired contact velocity $\boldsymbol{v}^*$, which is computed from the stiffness and damping parameters of the contact stabilization mechanism. $\boldsymbol{R}$ is a regularizing diagonal matrix with positive elements. When all inequality constraints are inactive, the substitution of the contact-space dynamics in Eq. (7) gives the solution for impulse $\boldsymbol{f}$ as

$$\boldsymbol{f} = \boldsymbol{R}^{-1}(\boldsymbol{v}^* - \boldsymbol{v}^+). \tag{8}$$

Substituting this in contact space dynamics, we get

$$\boldsymbol{v}^+ = \frac{\boldsymbol{v}^- + \boldsymbol{A}\boldsymbol{R}^{-1}\boldsymbol{v}^*}{1 + \boldsymbol{A}\boldsymbol{R}^{-1}}. \tag{9}$$

For current contact position $\boldsymbol{x}$, velocity $\dot{\boldsymbol{x}}$, and acceleration $\boldsymbol{a}_0$, the contact velocity before impulse is given as

$$\boldsymbol{v}^- = \dot{\boldsymbol{x}} + h\boldsymbol{a}_0. \tag{10}$$

For desired velocity, a virtual PD controller with gains $\boldsymbol{K}$ and $\boldsymbol{B}$, which causes the acceleration $-\boldsymbol{K}\boldsymbol{x} - \boldsymbol{B}\dot{\boldsymbol{x}}$, is considered. The desired contact velocity is given as

$$\boldsymbol{v}^* = \dot{\boldsymbol{x}} + h(-\boldsymbol{B}\dot{\boldsymbol{x}} - \boldsymbol{K}\boldsymbol{x}). \tag{11}$$

By substituting $\boldsymbol{v}^-$ and $\boldsymbol{v}^*$ in Eq. (9), contact velocity after impulse is obtained as

$$\boldsymbol{v}^+ = \dot{\boldsymbol{x}} + \frac{h}{\mathbf{1} + \boldsymbol{\epsilon}}(\boldsymbol{\epsilon}\boldsymbol{a}_0 - \boldsymbol{B}\dot{\boldsymbol{x}} - \boldsymbol{K}\boldsymbol{x}), \tag{12}$$

where,

$$\boldsymbol{\epsilon} = \frac{1}{\boldsymbol{A}\boldsymbol{R}^{-1}}. \tag{13}$$

The dynamics in the constraint space is rewritten as

$$a_1 + d(bv + kr) = (1 - d)a_0, \tag{14}$$

where,

$$d = \frac{1}{1 + \epsilon}. \tag{15}$$

Here, a_1 is the acceleration, v is the velocity, and r is the position or residual (defined as 0 in friction dimensions) in the constraint space. a_0 is the acceleration in the absence of the constraint force. The impedance $d \in (0, 1)$ corresponds to a constraint's ability to generate force, which is parameterized as a function of constraint violation r using the parameters of $\mathbf{solimp} = [d_0, d_{\text{width}}, \text{width}, \text{midpoint}, \text{power}]$. The impedance d is computed as

$$d = d_0 + y(d_{\text{width}} - d_0), \tag{16}$$

where,

$$y = \begin{cases} (\frac{1}{\text{midpoint}})^{(\text{power}-1)} \cdot (\frac{|r|}{\text{width}})^{\text{power}}, & \text{if } \frac{|r|}{\text{width}} \leq \text{midpoint}, \\ 1 - (\frac{1}{1-\text{midpoint}})^{(\text{power}-1)}. & \\ (1 - \frac{|r|}{\text{width}})^{\text{power}}, & \text{if } \frac{|r|}{\text{width}} > \text{midpoint} \\ & \text{and } \frac{|r|}{\text{width}} \leq 1, \\ 1, & \text{otherwise.} \end{cases} \tag{17}$$

In Eq. (14), k and b are the stiffness and damping of a virtual mass-spring-damper system, which are defined using parameters of $\mathbf{solref} = [\text{timeconst}, \text{dampratio}]$ as

$$k = \frac{d}{d_{\text{width}}^2} \cdot \text{stiffness}, \tag{18}$$

$$\text{stiffness} = \frac{1}{\text{timeconst}^2 \cdot \text{dampratio}^2}, \tag{19}$$

$$b = \frac{1}{d_{\text{width}}} \cdot \text{damping}, \tag{20}$$

$$\text{damping} = \frac{2}{\text{timeconst}}. \tag{21}$$

The solution for the contact force from the substitution of the contact-space dynamics, is given as

$$f = A^{-1}(-\boldsymbol{c}^T\boldsymbol{\delta}_{r,v} - d_0 a_0). \tag{22}$$

where, A is the mean of the diagonal elements of $\boldsymbol{J}\boldsymbol{M}^{-1}\boldsymbol{J}^T$. Here, the contact force depends not only on the bodies in contact but also on the robot's configuration. Therefore, the

penetration depth of the contact point between the foot and the terrain varies with the vertical position of the hip link of the robot. The expressions of $\boldsymbol{c}$ and $\boldsymbol{\delta}_{r,v}$ for the three cases of r are as follows:

- Case-1: $|r| \leq \text{midpoint} \cdot \text{width}$

$$\boldsymbol{c} = \begin{bmatrix} \frac{d_0^2 \cdot \text{stiffness}}{d_{\text{width}}^2} \\ \frac{(d_{\text{width}} - d_0) \cdot a_0}{\text{midpoint}^{\text{power}-1} \cdot \text{width}^{\text{power}}} \\ \frac{2d_0(d_{\text{width}} - d_0) \cdot \text{stiffness}}{d_{\text{width}}^2 \text{midpoint}^{\text{power}-1} \cdot \text{width}^{\text{power}}} \\ \frac{(d_{\text{width}} - d_0)^2 \cdot \text{stiffness}}{d_{\text{width}}^2 \cdot \text{midpoint}^{2\cdot\text{power}-2} \cdot \text{width}^{2\cdot\text{power}}} \\ \frac{d_0 \cdot \text{damping}}{d_{\text{width}}} \\ \frac{(d_{\text{width}} - d_0) \cdot \text{damping}}{d_{\text{width}} \text{midpoint}^{\text{power}-1} \cdot \text{width}^{\text{power}}} \end{bmatrix}, \tag{23}$$

$$\boldsymbol{\delta}_{r,v} = \begin{bmatrix} r \\ r^{\text{power}} \\ r^{\text{power}+1} \\ r^{2\cdot\text{power}+1} \\ v \\ r^{\text{power}} v \end{bmatrix}. \tag{24}$$

- Case-2: $\text{midpoint} \cdot \text{width} < |r| \leq \text{width}$

$$\boldsymbol{c} = \begin{bmatrix} \text{stiffness} \\ \frac{(d_{\text{width}} - d_0) \cdot a_0}{(1-\text{midpoint})^{\text{power}-1} \cdot \text{width}^{\text{power}}} \\ \frac{2(d_{\text{width}} - d_0) \cdot \text{stiffness}}{d_{\text{width}} (1-\text{midpoint})^{\text{power}-1} \cdot \text{width}^{\text{power}}} \\ \frac{(d_{\text{width}} - d_0)^2 \cdot \text{stiffness}}{d_{\text{width}}^2 \cdot (1-\text{midpoint})^{2\cdot\text{power}-2} \cdot \text{width}^{2\cdot\text{power}}} \\ \text{damping} \\ \frac{(d_{\text{width}} - d_0) \cdot \text{damping}}{d_{\text{width}} (1-\text{midpoint})^{\text{power}-1} \cdot \text{width}^{\text{power}}} \end{bmatrix}, \tag{25}$$

$$\boldsymbol{\delta}_{r,v} = \begin{bmatrix} r \\ -(\text{width} - r)^{\text{power}} \\ -r(\text{width} - r)^{\text{power}} \\ r(\text{width} - r)^{2\cdot\text{power}} \\ v \\ -v(\text{width} - r)^{\text{power}} \end{bmatrix}. \tag{26}$$

- Case-3: $|r| > \text{width}$

$$\boldsymbol{c} = \begin{bmatrix} \text{stiffness} \\ \text{damping} \end{bmatrix}, \tag{27}$$

$$\boldsymbol{\delta}_{r,v} = \begin{bmatrix} r \\ v \end{bmatrix}. \tag{28}$$

The force-deformation plot for the impact of a spherical ball (mass=1 kg, radius=1 cm, distance of center of ball from plane =2 cm) on a plane with default solver parameters is shown in Fig. 2. The effect of **solref** on the force-deformation behavior is also shown in the figure. The maximum deformation is shown to be significantly greater than the static equilibrium deformation of the ball. The contact force at the static equilibrium deformation is shown as a horizontal line in Fig. 2. Plane and box geometries

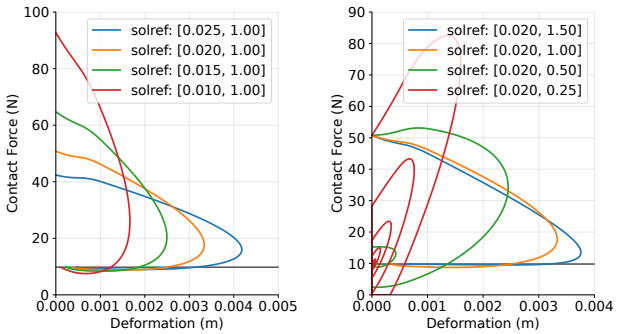

(a) Variation of time constant (b) Variation of damping ratio

Fig. 2: Force-deformation plot for collision of a ball on a plane with $\textbf{solimp} = [0.9, 0.95, 0.001, 0.5, 2]$

are interchangeably used to model the terrain in MuJoCo, however, incorrect contact penetration is observed in the sphere-box contact model of MuJoCo version 3.1.6, which was reported in the MuJoCo forum[1], and the developers have fixed this issue in version 3.2.7.

B. Identification of solver parameters

The static equilibrium deformation is crucial for robot footstep planning to avoid impact from the swing leg, and it can be used as a contact solver parameter. In solver parameters identification, the direct format is used, where the parameters in $\textbf{solref} = [-\text{stiffness}, -\text{damping}]$ are negative. For actual static equilibrium deformation r_{st} on deformable terrain at $d = d_{\text{midpoint}}$, the stiffness and damping is given as

$$\text{stiffness} = \frac{(1 - d_{\text{midpoint}}) g d_{\text{width}}^2}{r_{\text{st}} \cdot d_{\text{midpoint}}^2}, \tag{29}$$

$$\text{damping} = 2\sqrt{\text{stiffness}}. \tag{30}$$

Here, $d_{\text{midpoint}} = \text{midpoint} \cdot (d_0 + d_{\text{width}})$, $\text{width} = \frac{r_{\text{st}}}{\text{midpoint}}$ and $g = 9.81\,\text{m/s}^2$. For impact of a spherical ball (mass=1 kg, radius=1 cm, distance of center of ball from plane =2 cm) on a plane with $\textbf{solimp} = [0, 0.95, 0.02, 0.5, 2]$ and $\textbf{solref} = [-2060.1, -90.8]$, the force-deformation plot is shown in Fig. 3a. The static equilibrium deformation of the terrain is set to be equal to the radius of the ball. The calculated theoretical values of stiffness and damping give the desired deformation of the terrain, which can also be seen in the inverse dynamics plot of the ball with zero velocity and acceleration in Fig. 3b. The force-deformation behavior of the nonlinear Hunt-Crossley ($f_n = k_n \delta_n^{\frac{3}{2}} + c_n \delta_n^{\frac{3}{2}} \dot{\delta}_n$) contact model is also plotted in the figure.

The foot-terrain interaction on a deformable terrain with static equilibrium deformation of 6 mm and a damping ratio of 1.5 can be simulated by the impact of a box on a plane with $\textbf{solimp} = [0, 0.95, 0.012, 0.5, 2]$ and $\textbf{solref} = [-858.4, -87.9]$. The force-deformation plot is shown in Fig. 4a, and the inverse dynamics plot of the box with zero velocity and acceleration is shown in Fig. 4b.

[1]https://github.com/google-deepmind/mujoco/issues/2206

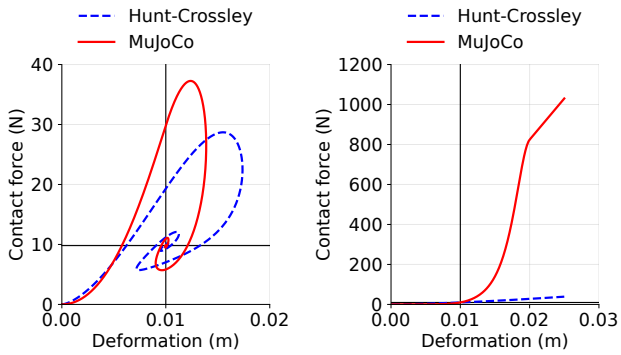

(a) Forward dynamics for collision of ball on plane

(b) Inverse dynamics of ball with zero velocity and acceleration

Fig. 3: Force-deformation plot for collision of ball on a plane with modified contact solver parameters (**solref** $= [-2060.1, -90.8]$ and **solimp** $= [0.0, 0.95, 0.02, 0.5, 2]$) of MuJoCo and Hunt Crossley Model ($k_n = 9810\,\mathrm{Nm}^{-3/2}, c_n = 19\,620\,\mathrm{Nsm}^{-5/2}$)

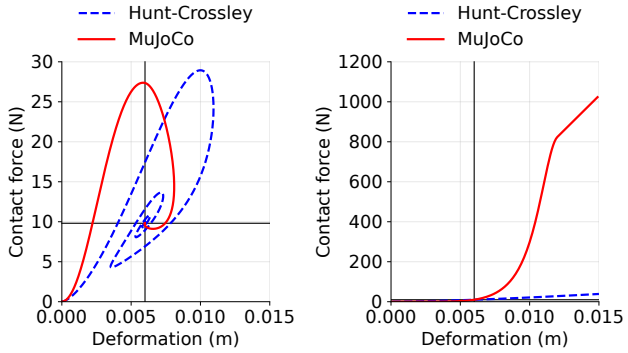

(a) Forward dynamics for collision of box on plane

(b) Inverse dynamics of box with zero velocity and acceleration

Fig. 4: Force-deformation plot for collision of box on a plane with modified contact solver parameters (**solref** $= [-858.4, -87.9]$ and **solimp** $= [0.0, 0.95, 0.012, 0.5, 2]$)

C. Humanoid robot on deformable terrain

A 22-DOF Kondo KHR-3HV humanoid robot is used for the inverse dynamics simulation in MuJoCo. The design parameters of the robot are given in Table I. The stiffness and damping values obtained theoretically from the box-plane collision model are $858.4\,\mathrm{s}^{-2}$ and $87.9\,\mathrm{s}^{-1}$, respectively, for the desired static equilibrium deformation of $6\,\mathrm{mm}$ due to the self-weight of the robot on deformable terrain with a damping ratio of 1.5. The contact force versus deformation of the terrain in inverse dynamics with zero joint velocities and accelerations is plotted in Fig. 5a. The static equilibrium deformation for the contact force to be equal to the weight of the robot is $8.66\,\mathrm{mm}$, which is significantly higher than the desired deformation of $6\,\mathrm{mm}$ due to the effect of robot configuration on the contact model[2]. Therefore, the stiffness and damping values at the contact point are numerically

[2]https://github.com/google-deepmind/mujoco/discussions/2669

TABLE I: Parameters of 22-DOF humanoid robot in MuJoCo

Mass	$1.762\,\mathrm{kg}$
Foot size	$50\,\mathrm{mm} \times 40\,\mathrm{mm}$
Position of COM	(0, 0.009, 0.213) m

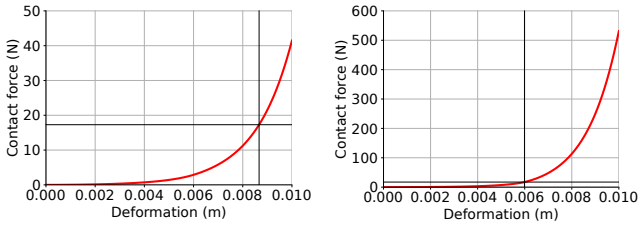

(a) Force-deformation plot for robot on terrain with **solref** $= [-858.4, -87.9]$

(b) Force-deformation plot for robot on terrain with **solref** $= [-11445.0, -320.9]$

Fig. 5: Inverse dynamics with zero joint velocities and accelerations of the robot on deformable terrain with **solimp** $= [0, 0.95, 0.012, 0.5, 2]$

increased to $11\,445.0\,\mathrm{s}^{-2}$ and $320.9\,\mathrm{s}^{-1}$, respectively, to get the desired deformation of the terrain in the inverse dynamics as shown in Fig. 5b.

IV. Conclusions

In this paper, we analyzed the solver parameters of MuJoCo for the sphere-plane and box-plane collision models. These parameters are estimated from the static equilibrium of the terrain and corrected using the robot's inverse dynamics to simulate walking on deformable terrain. In future work, we will study the identification of contact model parameters from experimental force-deformation data of the foot on deformable terrain, such as sand and grass.

References

[1] Q. Le Lidec, W. Jallet, L. Montaut, I. Laptev, C. Schmid, and J. Carpentier, "Contact models in robotics: a comparative analysis," *IEEE Transactions on Robotics*, 2024.

[2] X. Xiong, A. D. Ames, and D. I. Goldman, "A stability region criterion for flat-footed bipedal walking on deformable granular terrain," in *Proceedings of the 2017 IEEE/RSJ International Conference on Intelligent Robots and Systems (IROS)*. IEEE, 2017, pp. 4552–4559.

[3] G. Mesesan, J. Englsberger, G. Garofalo, C. Ott, and A. Albu-Schäffer, "Dynamic walking on compliant and uneven terrain using dcm and passivity-based whole-body control," in *Proceedings of the 2019 IEEE-RAS 19th International Conference on Humanoid Robots (Humanoids)*. IEEE, 2019, pp. 25–32.

[4] S. Gora, S. S. Gupta, and A. Dutta, "Energy-based footstep planning of biped on uneven deformable terrain using nonlinear inverted pendulum," *ASME Journal of Mechanisms and Robotics*, vol. 15, no. 5, p. 054502, 2023.

[5] ——, "Gait generation of a 10-degree-of-freedom humanoid robot on deformable terrain based on spherical inverted pendulum model," *ASME Journal of Mechanisms and Robotics*, vol. 17, no. 2, p. 021013, 2025.

[6] B. Acosta, W. Yang, and M. Posa, "Validating robotics simulators on real-world impacts," *IEEE Robotics and Automation Letters*, vol. 7, no. 3, pp. 6471–6478, 2022.

[7] S. Gora, S. S. Gupta, and A. Dutta, "Gait generation of 6-dof biped robot on inclined deformable terrain using nonlinear inverted pendulum," in *Proceedings of the 2023 6th International Conference on Advances in Robotics*, 2023, pp. 1–6.

[8] G. Gilardi and I. Sharf, "Literature survey of contact dynamics modelling," *Mechanism and machine theory*, vol. 37, no. 10, pp. 1213–1239, 2002.

[9] Y. F. Zheng, H. Wang, S. Li, Y. Liu, D. Orin, K. Sohn, Y. Jun, and P. Oh, "Humanoid robots walking on grass, sands and rocks," in *Proceedings of the 2013 IEEE Conference on Technologies for Practical Robot Applications (TePRA)*. IEEE, 2013, pp. 1–6.

[10] E. Todorov, T. Erez, and Y. Tassa, "Mujoco: A physics engine for model-based control," in *Proceedings of the 2012 IEEE/RSJ International Conference on Intelligent Robots and Systems*. IEEE, 2012, pp. 5026–5033.